Original Article

Evaluation of specific binding of [11C]TZ7774 to the receptor-interacting protein kinase 1 (RIPK1) in the brain

Takayuki Sakai[1], Takashi Yamada[1,2], Hiroshi Ikenuma[1], Aya Ogata[1,3], Masanori Ichise[1], Saori Hattori[1], Junichiro Abe[1], Mari Tada[4], Akiyoshi Kakita[4], Masaaki Suzuki[1], Kengo Ito[1], Takashi Kato[1], Shinichi Imamura[1], Yasuyuki Kimura[1]

[1]Department of Clinical and Experimental Neuroimaging, Center for Development of Advanced Medicine for Dementia, National Center for Geriatrics and Gerontology, Obu, Aichi, Japan; [2]Department of Human Life and Sciences Division of Health and Nutritional Science, Nagoya University of Economics, Nagoya, Japan; [3]Department of Pharmacy, Faculty of Pharmacy, Gifu University of Medical Science, Kani, Japan; [4]Department of Pathology, Brain Research Institute, Niigata University, Niigata, Japan

Abstract: Microglia, a type of immune cells of the central nervous system, play a critical role in the pathophysiology of neurodegenerative disorders including Alzheimer's disease (AD). Recently, efforts for drug discovery have focused on modifying the function of microglia to halt AD progression. One such effort targets a multifaceted kinase called receptor-interacting protein kinase 1 (RIPK1) that controls inflammation and cell death. Pharmaceutical inhibition of RIPK1 in microglia prevents their homeostatic status from transforming to disease-associated status. Thus, RIPK1 inhibitors can be a therapeutic agent for halting AD progression. Therefore, *in vivo* imaging of RIPK1 may be a useful biomarker of AD. Recently, a novel PET ligand, [11C]TZ7774, targeting RIPK1 was developed showing its ability to enter the brain and an increased uptake in the spleen of acute inflammation model mice. However, they have not yet shown direct evidence of specific binding of [11C]TZ7774 to RIPK1 in the brain. In this study, we replicated the synthesis of [11C]TZ7774 and examined its specific binding in the rat and human brain. Our studies with this ligand failed to detect sufficient specific binding of [11C]TZ7774 to RIPK1 in the brain neither by PET imaging with healthy and acute inflammation model rats, nor by autoradiography with healthy rat and human brain slices. Our results suggest that the RIPK1 ligand, [11C]TZ7774, is unlikely to be useful in humans. Future studies are warranted to develop more optimal radioligands for PET imaging of RIPK1.

Keywords: Receptor-interacting protein kinase 1, Alzheimer's disease, neuroinflammation, positron emission tomography

Introduction

Microglia, a type of immune cells of the central nervous system, play a critical role in the pathophysiology of neurodegenerative disorders including Alzheimer's disease (AD). In AD, phenotypically activated microglia that govern neural immunity are closely associated with senile plaques and neurofibrillary tangles [1]. The activated microglia have a significant impact on the formation of these pathological lesions and concurrent neurodegeneration [2]. Recently, efforts of drug discovery have focused on modifying the function of microglia to halt AD progression. One such effort targets a multifaceted kinase called receptor-interacting protein kinase 1 (RIPK1) that controls inflammation and cell death [3]. Pharmaceutical inhibition of RIPK1 in microglia prevents their homeostatic status from transforming to disease-associated status [4]. Thus, RIPK1 inhibitors can be a therapeutic agent for halting AD progression, as well as a potential *in vivo* imaging biomarker of AD.

To our knowledge, structurally different types of PET ligands for imaging of RIPK1 have been developed to date with high RIPK1 inhibitory activities (**Figure 1**). The first type of inhibitors are necrostatin (Nec-1) and Nec-1s. Necrostatin was the first RIPK1 inhibitor discovered by screening a chemical library containing 15,000 compounds [EC_{50} (Jurkat) = 494 nM] [5]. However, Nec-1 inhibits RIPK1 non-selectively due to its structural characteristics [6]. It also has low metabolic stability *in vivo*. Subsequent structure-activity relationship analysis discovered Nec-1s with an approximately 2.4-fold inhibitory activity of Nec-1 (EC_{50} = 206 nM) and improved metabolic stability [7]. The second type of inhibitor is GSK'963 [IC_{50}(RIPK1) = 29 nM], which effectively inhibited programmed necrosis of mouse and human cells at IC_{50} values of 1.0 nM and 4.0 nM, respectively [8]. The third type of inhibitor is benzoxazepine, 1 (TZ7774, **Figure 1**), exhibits a high pharmacological activity (K_i = 0.93 nM) and selectivity for RIPK1, and is also pharmacokinetically stable against RIPK1 [9].

The three structurally distinct PET ligands developed based on these RIPK1 inhibitors have been referred to as [18F]CNY-07, [11C]GG502, and [11C]TZ7774, respectively (**Figure 1**, bottom structures). The first two PET ligands, [18F]CNY-07 and [11C]GG502, were noted to be taken up into the mouse brain. However, their specific binding was not clearly demonstrated [10, 11]. In the report of [11C]TZ7774, this ligand was used in mice and macaques, showing its ability to take up into the brain [12]. Their biodistribution study demonstrated that ligand uptake was increased in the spleen of LPS-induced acute inflammation model mice. These findings suggested that this ligand
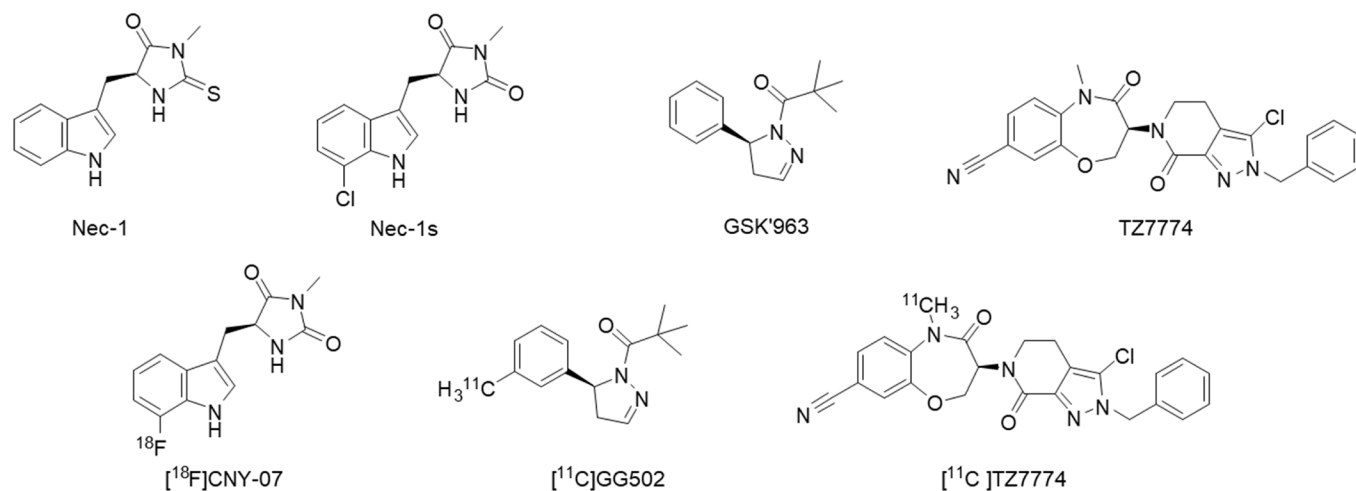
Figure 1. Structures of typical RIPK1-targeted inhibitors and PET ligands so far developed.

could be used as a PET radioligand for imaging RIPK1 *in vivo* in animals. However, they have not shown any direct evidence of specific binding of [^{11}C]TZ7774 to RIPK1 in the brain. In this study, we evaluated it's specific binding to RIPK1 by PET in the rat brain and additionally by autoradiography of brain sections of rats and humans. We selected [^{11}C]TZ7774 for testing because it has a much higher potential to exhibit specific binding to RIPK1, given its greater potency compared to the others, and no direct evidence of its specific binding has yet been demonstrated.

Methods

Chemicals and synthesis

The precursor compound (TZ7790) and standard compound (TZ7774) were synthesized according to the method to synthesize compound **22** (TZ7774) reported by Yoshikawa et al. [9] (Scheme S1). The structure of [^{11}C]TZ7774 was achieved by reacting TZ7790 [^{11}C]CH$_3$I under basic conditions [12] (Scheme S2). The structure of [^{11}C]TZ7774 was identified by comparing its HPLC retention time to that of the standards, TZ7774 (Figure S1). Details are described in the Supplementary Information.

Animals

The current PET imaging study utilized male F344/NSlc rats, 7 weeks old, obtained from Japan SLC, Inc., Hamamatsu, Japan. The animals involved in this study were housed and treated according to the National Research Council's Guide for the Care and Use of Laboratory Animals and our institution's regulations. The experimental protocols received approval from the Animal Ethics Committee of the National Center for Geriatrics and Gerontology.

Intracerebral administration of LPS - induction of neuro-inflammation

Two male F344/NSlc rats, 9 weeks old and weighing 146-156 g, were anesthetized using intraperitoneal adminis-

tration of medetomidine hydrochloride (0.325 mg/kg), midazolam (2.0 mg/kg), butorphanol tartrate (2.5 mg/kg) and isoflurane anesthesia (~2.0%). After anesthesia, intracerebral administration of lipopolysaccharide (LPS, Escherichia coli (O55:B5), Merck, USA) was done by using a stereotaxic instrument (NARISHIGE, Tokyo, Japan). The rat's head was precisely positioned in the apparatus, and a midline sagittal incision was made in the scalp. Intracerebral administration was carried out in the right striatum at these coordinates: anteroposterior (AP) = -0.23 mm, mediolateral (ML) = 1.0 mm, and dorsoventral (DV) = -2.5 mm. Then, the LPS (1 mg/80 µL) was dissolved in saline and administered via intracerebral injection using a micro-syringe at an infusion rate of 0.5 µL/min, with a total volume of 2 µL per animal. After administration, the incised scalp was sutured. Rats were carefully observed until recovery; after 7 days, they were used for PET imaging experiments, after which the brains were removed and used for the following western blot analysis.

PET brain imaging in rats

To evaluate *in vivo* specific binding of [^{11}C]TZ7774, blocking studies were performed using two blocking agents TZ7774 and GSK'963 in male F344/NSlc rats 9 weeks old, weighing 146-157 g. The rats were given an intravenous administration of 1.0 mg/kg of TZ7774 or GSK'963 (AOBIOUS, USA) as a blocking agent 30 minutes prior to the injection of [^{11}C]TZ7774. PET imaging was performed for 60 minutes on the FX3200 small animal PET scanner (TriFoil Imaging, CA, USA) following the administration of [^{11}C]TZ7774 (23.6-32.7 MBq, 0.27-0.69 nmol) through the tail vein. The procedure was performed under isoflurane anesthesia at approximately 2.0%. For the LPS experiments, two rats that received LPS injections were subjected to a 120 minutes PET scan utilizing a PET scanner designed for small animals following the administration of [^{11}C]TZ7774 (20.9-36.7 MBq, 0.19-0.34 nmol) through the tail vein while under approximately 2.0% iso-

flurane anesthesia. All PET images were processed with the 3D ordered subset expectation maximization (OSEM) algorithm, employing four subsets and twenty iterations. The resulting voxel dimensions was 0.6 × 0.5 × 0.5 mm, and the resolution was 0.92 mm at full width at half maximum (FWHM) in the middle of the field of view.

Autoradiography

Postmortem human brain samples were acquired through autopsies conducted at Niigata University's Brain Research Institute, from a patient who had colon cancer and liver metastases. Wild-type rat brains were swiftly removed and promptly frozen using powdered solid form of carbon dioxide. For in vitro autoradiography, fresh frozen sections of 7 μm thickness were prepared for human samples and 20 μm thickness for rat samples. Initially, sections were incubated in bovine serum for 30 minutes, followed by incubation in bovine serum containing [^{11}C]TZ7774 at concentrations of 5.1 nM for human samples, 15.7 nM for rat samples for the TZ7774 blocking study, and 55.6 nM for both samples for the GSK'963 blocking study. This incubation took place at 30°C for 30 minutes, with or without the addition of 10 μM of either TZ7774 or GSK'963 as blocking agents. After incubation, samples were washed twice with cold serum (4°C) for 2 minutes each and then immersed in cold water (4°C) for 10 seconds. Subsequently, the sections were dried using cold air and placed onto an imaging plate (BAS-SR2040, Fuji Film, Tokyo, Japan). The autoradiograms were imaged using a Typhoon FLA9500 scanner (GE Healthcare, IL, USA).

Western blot analysis

The preparation of samples containing 6 μg of protein, electrophoresis, and transfer to membrane followed our previous method [13]. The membranes were left overnight at 4°C in the presence of primary antibodies. The antibodies used included a monoclonal antibody specific to rabbit RIPK1 (RIP (D94C12) XP® Rabbit mAb, 1:250, Cell Signaling Technology, Inc., USA) and a polyclonal antibody against mouse β-actin (1:5000; Proteintech, USA). Following this, the membranes underwent additional incubation with secondary antibodies: goat anti-mouse IgG conjugated with peroxidase (1:3000; Abcam, USA) and goat anti-rabbit IgG conjugated with peroxidase (1:3000; Proteintech, USA). Then, immunoreactive bands were visualized using enhanced chemiluminescence (Thermo Scientific, USA). The bands were visualized utilizing FluorChem™ R (bio-techne ProteinSimple, Japan) and analyzed for densitometry with software (ImageJ, The National Institutes of Health, Bethesda, USA). Optical density values, normalized to β-actin, were compared between the right and left striata.

Results

We synthesized TZ7774 and TZ7790 (Scheme S1) as the precursor compound of radiolabeling and the non-radiolabeled standard material, respectively (detailed in Syntheses of intermediate compounds section in Supplementary Information). Then, [^{11}C]TZ7774 was synthesized with a molar activity of 137.8 ± 54.3 GBq/μmol and radiochemical purity of >99.9% at the end of radiosynthesis (detailed in Radiochemistry in Supplementary Information).

After intravenous administration of [^{11}C]TZ7774 to rats, brain radioactivity peaked at 2 min after bolus injection of [^{11}C]TZ7774 (SUV 1.2-1.5), rapidly declined for 10 min, and then slowly washed out for the rest of the scan period (**Figures 2A-E**, S2A-E). In the blocking study, neither TZ7774 or GSK'963 significantly changed the time-activity curve of [^{11}C]TZ7774 from the baseline. With TZ7774 as a blocking agent, radioactivity in the cerebellum decreased by 14% from the baseline on the average during 30 to 60 min (**Figure 2E**). However, with GSK'963, another RIPK1 inhibitor sharing the same binding site as TZ7774, radioactivity in the cerebellum increased by 24% (Figure S2E), suggesting that TZ7774 may have off-target binding in the cerebellum.

To examine whether [^{11}C]TZ7774 can detect increased RIPK1 density in the brain, acute neuroinflammation was induced by injecting lipopolysaccharide (LPS) into the rat right striatum. Western blotting confirmed increased RIPK1 concentration by two folds in the right striatum compared to the left (Figure S3). PET imaging showed only slight increases of radioactivity in the right striatum, the epicenter of the inflammation (**Figure 3**).

Autoradiography was then performed to evaluate specific binding of [^{11}C]TZ7774. In healthy rats, radioactivity was uniformly distributed in the rat brain and ~22% of radioactivity decreased with TZ7774 (**Figure 4A**). In human brain sections, radioactivity decreased by 33% with TZ7774 (**Figure 4B**). In contrast, GSK'963 did not change radioactivity in rat and human brain sections (Figure S4). The difference in the blocking effect between TZ7774 and GSK'963 maybe due to the fact that the former is a homologous competitor of [^{11}C]TZ7774.

Discussion

In this study, *in vivo* and *in vitro* experiments showed that specific binding of [^{11}C]TZ7774 to RIPK1 has not been reliably detected. We found slight blocking effects with homologues blocking by TZ7774, but the existence of specific binding selective to RIPK1 has not been confirmed by the blocking with GSK'963. The difference in the blocking effect between TZ7774 and GSK'963 maybe due to the fact that the former is a homologous competitor of [^{11}C]TZ7774.

This study explored a different approach to TZ7790 synthesis by employing the method of Yoshikawa et al. [9]. The amide intermediate synthesis process used iron powder to reduce the nitro group of intermediate **4** and hydro-
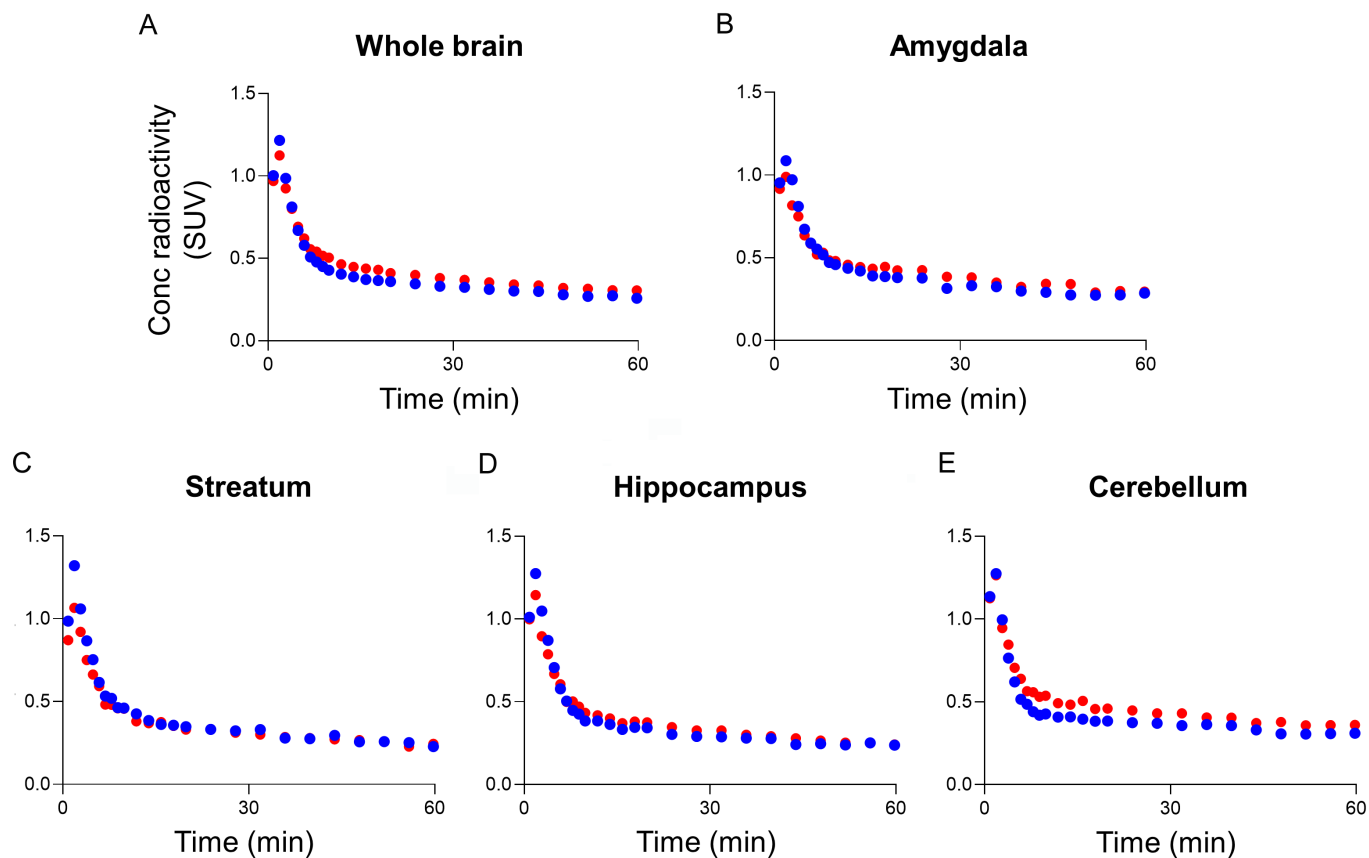
Figure 2. PET imaging of [^{11}C]TZ7774 in rats includes averaged time-activity curves for different brain regions. The regions analyzed are: whole brain (A), amygdala (B), striatum (C), hippocampus (D), and cerebellum (E). The data compare the results after injection of [^{11}C]TZ7774 with (blue circles) and without (red circles) the administration of 1 mg/kg of TZ7774 as a blocking agent.
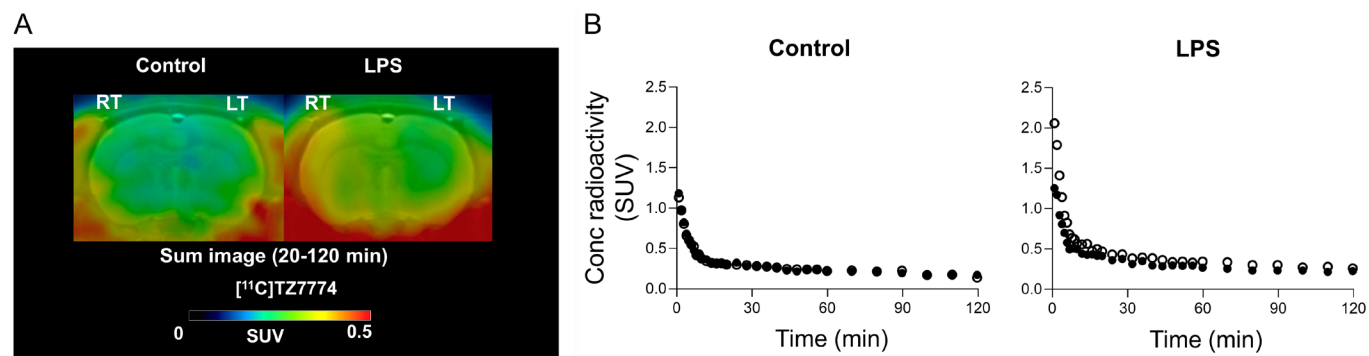

Figure 3. PET imaging was conducted on rats injected with [^{11}C]TZ7774, both with and without LPS injection in the right striatum. A. Brain PET images averaged between 20 and 60 minutes after injection, depict coronal slices with standardized uptake values superimposed on a template MR image. B. Averaged time-activity curves of the left (LT, filled circle) and right (RT, open circle) striatum after [^{11}C]TZ7774 injection are shown for rats with and without LPS injection in the right striatum.

chloric acid to deprotect the Boc group of intermediate **6**, both of which the yield was good. Details are described in the Supplementary Information. The [^{11}C]methylation conditions reported for the synthesis of [^{11}C]TZ7774 used NaOH powder as a base at 80°C for 5 minutes. On the other hand, our study showed that the use of NaOH resulted in hydrolysis of TZ7790 and a higher percentage of side-reactants. Therefore, we selected cesium carbonate, which is less hygroscopic than NaOH, as the base. As

expected, the reaction proceeded smoothly at room temperature and TZ7774 was obtained in 87% yield. Under these reaction conditions, [^{11}C]TZ7774 was successfully synthesized and sufficient amount of the radioligand was obtained to proceed with PET studies.

The study originally reported [^{11}C]TZ7774 by Huang et al. did not examine its specific binding [12]. Therefore, we investigated specific binding by performing *in vivo* and *in*
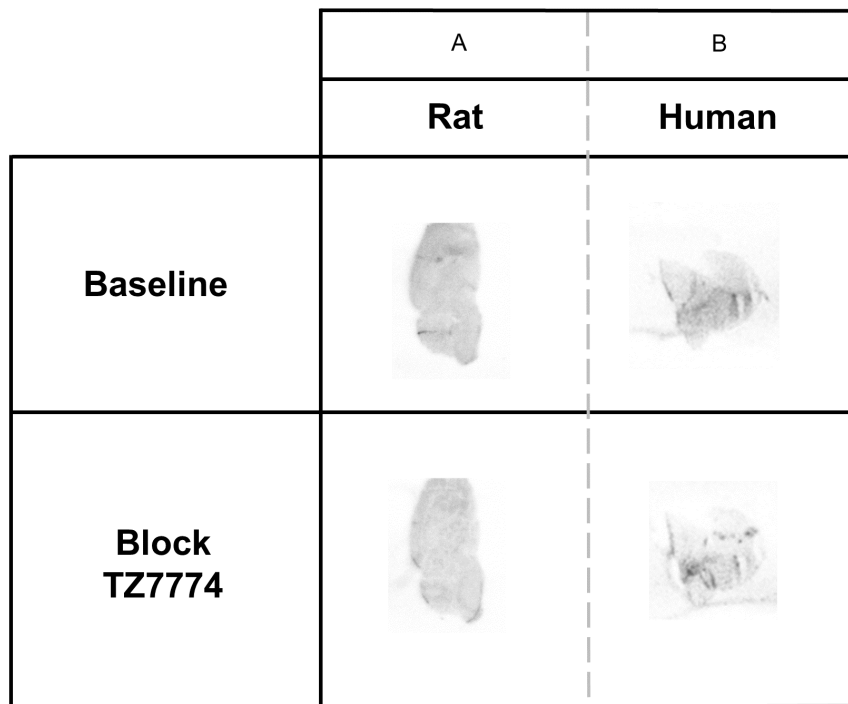
	A	B
	Rat	**Human**
Baseline		
Block TZ7774		

Figure 4. Autoradiography of sagittal section of healthy rat (A) and frontal sections of healthy human (B), with or without addition of TZ7774 (10 μM) as a blocking agent.

vitro blocking studies with TZ7774 itself and GSK'963, another RIPK1 inhibitor sharing the same binding pocket with TZ7774 [12]. Intravenous administration of [11C]TZ7774 to healthy rats resulted in uptake in the brain, and slight blocking effects were observed with homologous blocking with TZ7774, but no blocking effects with GSK'963. These observations were consistently shown in the autoradiography in rat and human brains. The radioactivity showed a slight blocking effect in rat and human brain sections by homologous blocking with TZ7774, but no blocking effects with GSK'963. While the blocking dose of 1 mg/kg in the PET study might be insufficient to achieve the necessary brain concentration for blocking RIPK1, our autoradiography employed a significantly higher concentration (10 μM) of the blocking agent. Thus, specific binding of [11C]TZ7774 to RIPK1 appears not sufficient for PET imaging in the rat and human brain. The increase in radioactivity in the cerebellum with GSK'963 may suggest off-target binding, which needs further investigation. However, TZ7774 has been shown to be highly selective in tests involving multiple target panels [9], suggesting that the likelihood of off-target binding is very low. In a rat model of acute inflammation, Western blot confirmed a solid increase in RIPK1. Nevertheless, PET imaging showed only small increase in the striatum of acute inflammation. These indicate that [11C]TZ7774 is not suitable as a PET imaging ligand to observe RIPK1 densities in rat and human brain.

A possible explanation for the poor PET visualization of [11C]TZ7774's specific binding, despite its high *in vitro* binding affinity for RIPK1 (pK_i = 9.0) [9], is the very low expression level of RIPK1 in human brain (0.5 parts per million [ppm]) [13]. By contrast, the translocator protein 18 kDa (TSPO), a well-known target for PET imaging of neuroinflammation, is expressed at a much higher level (7.5 ppm), 15 times greater than that of RIPK1 [14]. Therefore, PET ligands for TSPO, having similar binding affinity values to TZ7774, can demonstrate TSPO specific binding by PET [15].

Although it is possible that specific binding could have been detectable in AD patients given the high RIPK1 levels reported [4]. The acute inflammation model induced by LPS does not fully replicate the complex inflammatory processes seen in AD, including potential differences like increased cerebral blood flow. Regardless, we used this model to assess the ability of [11C]TZ7774 to detect specific binding to RIPK1 in the brain of the acute inflammation model, whose RIPK1 levels were shown to be increased by Western blot. Since we did not observe increased radioactivity in this model, we believe that [11C]TZ7774 may not show specific binding in AD either.

Thus, to detect specific binding of RIPK1 in the brain, PET ligands must possess even higher binding affinity for RIPK1 than does TZ7774. Achieving this level of performance may not be possible with reversibly binding small molecules. One approach would be to develop PET ligands that induce irreversible binding to RIPK1. Another possible approach is to use macromolecular substances, such as antibodies targeting RIPK1 with extremely high binding affinity for RIPK1.

Conclusions

In our study, specific binding of [11C]TZ7774 to RIPK1 has not been reliably detected. Future studies appear warranted to develop more suitable radioligands for PET imaging of RIPK1.

Acknowledgements

Disclosure of conflict of interest

None.

Address correspondence to: Dr. Yasuyuki Kimura, Department of Clinical and Experimental Neuroimaging, Center for Development of Advanced Medicine for Dementia, National Center for Geriatrics and Gerontology, 7-430 Morioka-cho, Obu, Aichi 474-8511, Japan. Tel: +81-562462311; Fax: +81-562446596; E-mail: yazkim@ncgg.go.jp

References

[1] Ohm DT, Fought AJ, Martersteck A, Coventry C, Sridhar J, Gefen T, Weintraub S, Bigio E, Mesulam MM, Rogalski E and Geula C. Accumulation of neurofibrillary tangles and activated microglia is associated with lower neuron densities in the aphasic variant of Alzheimer's disease. Brain Pathol 2021; 31: 189-204.

[2] Mandrekar-Colucci S and Landreth GE. Microglia and inflammation in Alzheimer's disease. CNS Neurol Disord Drug Targets 2010; 9: 156-167.

[3] Mifflin L, Ofengeim D and Yuan J. Receptor-interacting protein kinase 1 (RIPK1) as a therapeutic target. Nat Rev Drug Discov 2020; 19: 553-571.

[4] Ofengeim D, Mazzitelli S, Ito Y, DeWitt JP, Mifflin L, Zou C, Das S, Adiconis X, Chen H, Zhu H, Kelliher MA, Levin JZ and Yuan J. RIPK1 mediates a disease-associated microglial response in Alzheimer's disease. Proc Natl Acad Sci U S A 2017; 114: E8788-E8797.

[5] Degterev A, Hitomi J, Germscheid M, Ch'en IL, Korkina O, Teng X, Abbott D, Cuny GD, Yuan C, Wagner G, Hedrick SM, Gerber SA, Lugovskoy A and Yuan J. Identification of RIP1 kinase as a specific cellular target of necrostatins. Nat Chem Biol 2008; 4: 313-321.

[6] Chen L, Zhang X, Ou Y, Liu M, Yu D, Song Z, Niu L, Zhang L and Shi J. Advances in RIPK1 kinase inhibitors. Front Pharmacol 2022; 13: 976435.

[7] Takahashi N, Duprez L, Grootjans S, Cauwels A, Nerinckx W, DuHadaway JB, Goossens V, Roelandt R, Van Hauwermeiren F, Libert C, Declercq W, Callewaert N, Prendergast GC, Degterev A, Yuan J and Vandenabeele P. Necrostatin-1 analogues: critical issues on the specificity, activity and in vivo use in experimental disease models. Cell Death Dis 2012; 3: e437.

[8] Berger SB, Harris P, Nagilla R, Kasparcova V, Hoffman S, Swift B, Dare L, Schaeffer M, Capriotti C, Ouellette M, King BW, Wisnoski D, Cox J, Reilly M, Marquis RW, Bertin J and Gough PJ. Characterization of GSK'963: a structurally distinct, potent and selective inhibitor of RIP1 kinase. Cell Death Discov 2015; 1: 15009.

[9] Yoshikawa M, Saitoh M, Katoh T, Seki T, Bigi SV, Shimizu Y, Ishii T, Okai T, Kuno M, Hattori H, Watanabe E, Saikatendu KS, Zou H, Nakakariya M, Tatamiya T, Nakada Y and Yogo T. Discovery of 7-Oxo-2,4,5,7-tetrahydro-6H-pyrazolo[3,4-c]pyridine derivatives as potent, orally available, and brain-penetrating receptor interacting protein 1 (RIP1) kinase inhibitors; analysis of structure-kinetic relationships. J Med Chem 2018; 61: 2384-409.

[10] Lan Y, Bai P, Liu Y, Afshar S, Striar R, Rattray AK, Meyer TN, Langan AG, Posner AM, Shen S, Tanzi RE, Zhang C and Wang C. Visualization of receptor-interacting protein kinase 1 (RIPK1) by brain imaging with positron emission tomography. J Med Chem 2021; 64: 15420-15428.

[11] Ikenuma H, Ogata A, Koyama H, Ji B, Ishii H, Yamada T, Abe J, Seki C, Nagai Y, Ichise M, Minamimoto T, Higuchi M, Zhang MR, Kato T, Ito K, Suzuki M and Kimura Y. Synthesis and evaluation of a novel PET ligand, a GSK'963 analog, aiming at autoradiography and imaging of the receptor interacting protein kinase 1 in the brain. EJNMMI Radiopharm Chem 2023; 8: 31.

[12] Huang T, Gu J, Jiang H, Liang Q, Perlmutter JS and Tu Z. Radiosynthesis and characterization of a carbon-11 PET tracer for receptor-interacting protein kinase 1. Nucl Med Biol 2022; 110-111: 18-27.

[13] Sakai T, Hattori S, Ogata A, Yamada T, Abe J, Ikenuma H, Ichise M, Suzuki M, Ito K, Kato T and Kimura Y. Noradrenaline transporter PET reflects neurotoxin-induced noradrenaline level decrease in the rat hippocampus. EJNMMI Res 2023; 13: 82.

[14] Huang Q, Szklarczyk D, Wang M, Simonovic M and von Mering C. PaxDb 5.0: curated protein quantification data suggests adaptive proteome changes in yeasts. Mol Cell Proteomics 2023; 22: 100640.

[15] Doorduin J, Klein HC, Dierckx RA, James M, Kassiou M and de Vries EF. [^{11}C]-DPA-713 and [^{18}F]-DPA-714 as new PET tracers for TSPO: a comparison with [^{11}C]-(R)-PK11195 in a rat model of herpes encephalitis. Mol Imaging Biol 2009; 11: 386-398.

Supplementary Information

Experimental section

Chemicals

All commercially obtained solvents and reagents were used as received without further purification. All reactions were conducted in a nitrogen atmosphere. Normal-phase thin-layer chromatography (TLC) was performed using Silica gel 60 F254 (1.05715.0009, Merck, USA), reagent grade solvent, and UV light (254 nm) or phosphomolybdic acid as visualization reagent. Column chromatography was carried out using silica gel (AP-300S Taiko-shoji) with solvent mixtures as specified. ^{1}H and spectra were acquired for samples dissolved in $CDCl_3$ or DMSO-d_6 using the JEOL JNM-ECA500 spectrometer operating at a frequency of 500 MHz for ^{1}H, with tetramethylsilane (TMS) used as an internal reference. ^{1}H NMR spectra chemical shifts are given as δ values (ppm), with the singlet of tetramethylsilane set at 0 ppm as the reference. Splitting patterns are indicated as follows: s for singlet, d for doublet, t for triplet, dd for doublet of doublets, ddd for doublet of doublet of doublets, td for triplet of doublets, m for multiplet. Electrospray ionization (ESI)-mass spectrometry measurements were conducted using the shimadzu LC-MS2020 spectrometer. The solvents were removed by evaporation under reduced pressure using a rotary evaporator.

Synthesis of intermediate compounds
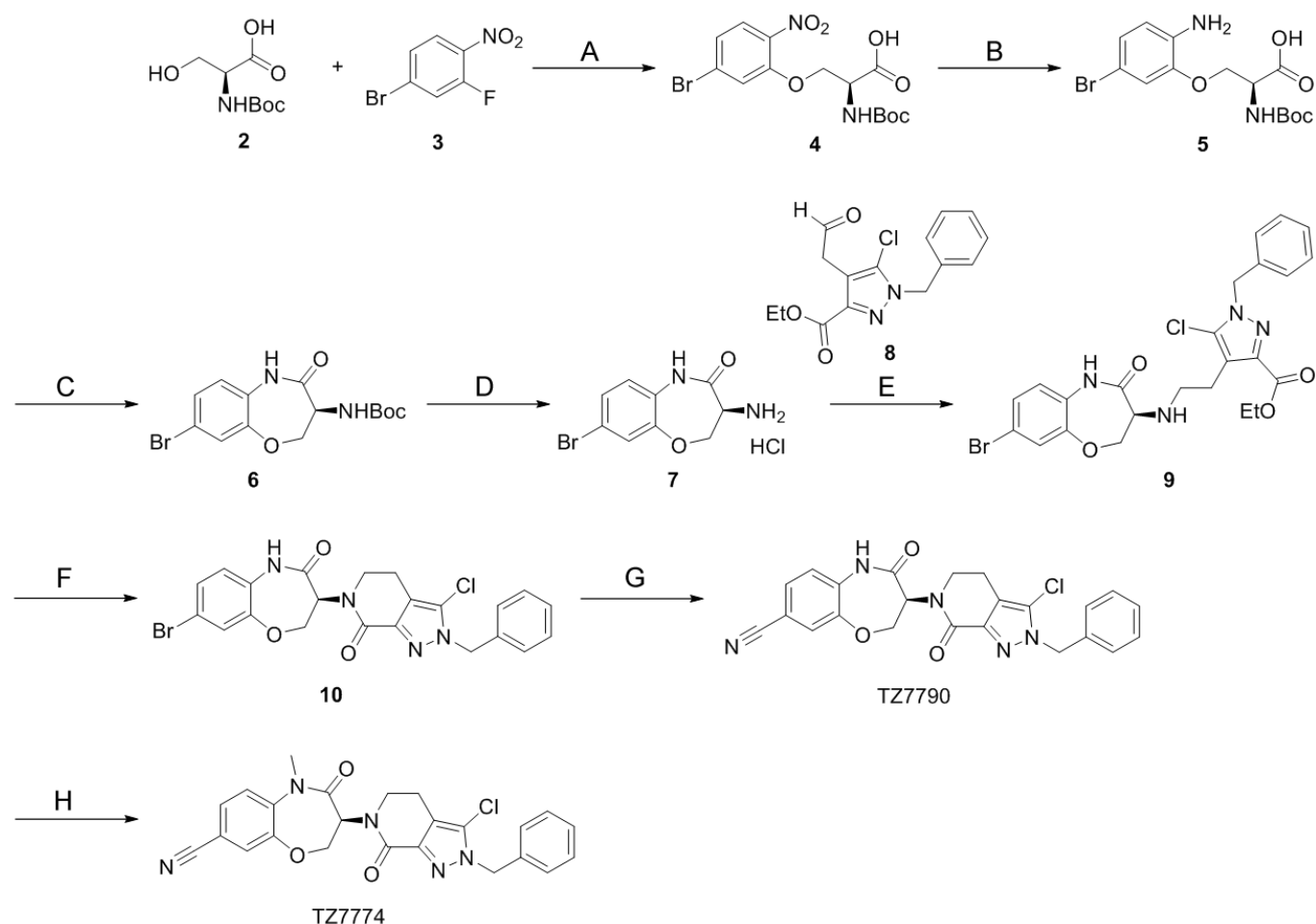
Scheme S1. Synthesis of standard compound TZ7774 and precursor Dm-NCGG501. Agents and reaction conditions: (A) NaH (60%), DMF, 0°C to rt; (B) Fe, H_2O, EtOH, 80°C; (C) HATU, TEA, DMSO, rt; (D) 4 M HCl/EtOAc, 0°C to rt; (E) 5, 2-picoline boran, 8, HOAc, MeOH, rt; MeOH, rt; (F) AlMe$_3$, toluene, 0°C to 100°C; (G) Zn(CN)$_2$, Pd(PPh$_3$)$_4$, DMF, 100°C, under Ar; (H) Cs$_2$CO$_3$, MeI, DMF, 0°C to rt.

(S)-3-(5-Bromo-2-nitrophenoxy)-2-((tert-butoxycarbonyl)amino)propanoic Acid (4) [1]

Following the method by Huang et al. [1], 4 was obtained, yielding 26 mg (6.4%). ^{1}H NMR (500 MHz, DMSO-d_6): δ = 1.38 (9H, s), 4.33-4.49 (3H, m), 7.12 (^{1}H, J = 8.0 Hz, d), 7.35 (^{1}H, dd, J = 8.5, J = 2.0 Hz), 7.65 (^{1}H, J = 2.0 Hz, d), 7.84 (^{1}H, J = 9.5 Hz, d); LRMS (ESI-): m/z [M+H]$^-$: 403.

(S)-3-(2-Amino-5-bromophenoxy)-2-((tert-butoxycarbonyl)amino)propanoic Acid (5) [1]

Following the method by Yoshikawa et al. [1], 5 was obtained, yielding 19 mg (88%). LRMS (ESI-): m/z [M+H]$^-$: 373.

(S)-tert-Butyl (8-Bromo-4-oxo-2,3,4,5-tetrahydrobenzo[b][1,4]oxazepin-3-yl)carbamate (6) [1]

Following the method by Y Huang et al. [1], 6 was obtained, yielding 10 mg (67%). ^{1}H NMR (500 MHz, DMSO-d_6): δ = 1.36 (9H, s), 4.24-4.40 (3H, m), 7.00-7.06 (^{1}H, m), 7.14 (^{1}H, J = 8.5 Hz, d), 7.29-7.36 (2H, m), 10.02 (^{1}H, s); LRMS (ESI-): m/z [M+H]$^-$: 355.

(S)-3-Amino-8-bromo-2,3-dihydrobenzo[b][1,4]oxazepin-4(5H)-one Hydrochloride (7) [1]

Following the method by Huang et al. [1], 7 was obtained, yielding 35 mg (quant). LRMS (ESI+): m/z [M+H]$^+$: 257.

(S)-Ethyl 1-Benzyl-5-chloro-4-(2-((7-cyano-5-methyl-4-oxo2,3,4,5-tetrahydrobenzo[b][1,4]oxazepin-3-yl)amino)ethyl)-^{1}H-pyrazole3-carboxylate (9) [1]

Following the method by Huang et al. [1], 9 was obtained, yielding 42 mg (64%). ^{1}H NMR (500 MHz, CDCl$_3$): δ = 1.38 (3H, J = 8.5 Hz, t), 2.59-2.67 (^{1}H, m), 2.75-2.96 (3H, m), 3.59 (^{1}H, dd, J = 10.5, 6.0 Hz), 4.07-4.15 (^{1}H, m), 4.31-4.44 (3H, m), 5.40 (2H, s), 6.81 (^{1}H, J = 8.5 Hz, d), 7.15-7.34 (6H, m), 7.40 (^{1}H, s); LRMS (ESI-): m/z [M-H]$^-$: 545.

(S)-3-(2-Benzyl-3-chloro-7-oxo-4,5-dihydro-2H-pyrazolo[3,4-c]pyridin-6(7H)-yl)-8-bromo-5-methyl-2,3-dihydrobenzo[b][1,4]oxazepin-4(5H)-one (10) [1]

Following the method by Huang et al. [1], 10 was obtained, yielding 50 mg (68%). ^{1}H NMR (400 MHz, CDCl$_3$): δ = 2.68-2.77 (^{1}H, m), 2.89-2.99 (^{1}H, m), 3.64-3.74 (^{1}H, m), 4.45 (^{1}H, dd, J = 11.0, J = 5.2 Hz), 4.61 (^{1}H, dd, J = 11.4, J = 2.4 Hz), 5.36-5.50 (3H, m), 6.79 (^{1}H, d, J = 8.8), 7.18 (^{1}H, dd, J = 9.0, J = 2.2 Hz), 7.27-3.36 (5H, m), 7.60 (^{1}H, s); LRMS (ESI+): m/z [M-H]$^+$: 501.
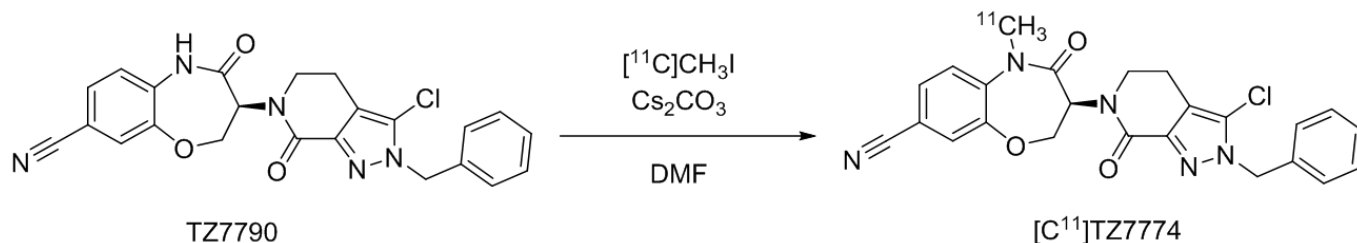
(3S)-3-(2-Benzyl-3-chloro-7-oxo-2,4,5,7-tetrahydro-6H-pyrazolo[3,4-c]pyridin-6-yl)-4-oxo-2,3,4,5-tetrahydro-1,5-benzoxazepine-8-carbonitrile (TZ7790) [1]

Following the method by Huang et al. [1], TZ7790 was obtained, yielding 11 mg (27%). ^{1}H NMR (500 MHz, CDCl$_3$): δ = 2.76 (^{1}H, dt, J = 10.5, 6.6 Hz), 2.93 (^{1}H, q, J = 7.9 Hz), 3.78 (2H, dd, J = 7.5, 5.5 Hz), 4.49 (^{1}H, dd, J = 12.0, 4.5 Hz), 4.66(^{1}H, dd, J = 12.0, 4.0 Hz), 5.19 (^{1}H, br s), 5.40 (2H, s), 6.96 (^{1}H, d, J = 8.0 Hz), 7.28-7.36 (6H, m), 7.38 (^{1}H, d, J = 2.0 Hz), 7.73 (^{1}H, br s); LRMS (ESI+): m/z [M-H]$^+$: 448.

(3S)-3-(2-Benzyl-3-chloro-7-oxo-2,4,5,7-tetrahydro-6H-pyrazolo[3,4-c]pyridin-6-yl)-5-methyl-4-oxo-2,3,4,5-tetrahydro-1,5-benzoxazepine8-carbonitrile (TZ7774) [2]

Following the method by Yoshikawa et al. [2], TZ7774 was obtained, yielding 8.6 mg (87%). to give TZ7774 (8.6 mg, 87%) as a white solid. ^{1}H NMR (500 MHz, CDCl$_3$): δ = 2.69 (^{1}H, dt, J = 16.0, 4.8 Hz), 3.05 (^{1}H, ddd, J = 15.5, 10.4, 5.2 Hz), 3.40 (3H, s), 3.52-3.60 (^{1}H, m), 4.174.25 (^{1}H, m), 4.45 (^{1}H, dd, J = 10.3, 8.3), 4.69 (^{1}H, dd, J = 12.0, 10.0 Hz), 5.40 (^{1}H, s) 5.90 (^{1}H, dd, J = 11.5, 8.0 Hz), 7.24-7.37 (6H, m), 7.48 (^{1}H, d, J = 2.0 Hz), 7.57 (^{1}H, d, J = 8.3, 1.8 Hz); LRMS (ESI+): m/z [M-H]$^+$: 461.

Radiochemistry

Radio-labeling was conducted according to the previously reported method [3].

Scheme S2. Radiosynthesis of [^{11}C]TZ7774. TZ7790 was methylated with [^{11}C]CH$_3$I with Cs$_2$CO$_3$ in DMF DMF at rt for 10 min.

(3S)-3-(2-Benzyl-3-chloro-7-oxo-2,4,5,7-tetrahydro-6H-pyrazolo[3,4-c]pyridin-6-yl)-5-[^{11}C]methyl-4-oxo-2,3,4,5-tetrahydro-1,5-benzoxazepine8-carbonitrile ([^{11}C]TZ7774)

(3S)-3-(2-Benzyl-3-chloro-7-oxo-2,4,5,7-tetrahydro-6H-pyrazolo[3,4-c]pyridin-6-yl)-4-oxo-2,3,4,5-tetrahydro-1,5-benzoxaz-epine-8-carbonitrile (TZ7790) (0.50-2.6 mg, 1.05-5.44 µmol) was dissolved in DMF (300 µL), added potassium carbonate (20 mg, 145 µmol). [^{11}C] methyl iodide was prepared following general methods, transferred to the reaction vial and heated to rt for 10 min. The reaction mixture was purified by HPLC (column: CAPCELL PAK C18, UG120, 10 mmI. D. × 250 mm, UV = 260 nm) eluting with a 55% CH$_3$CN in 0.1% formic acid at a flow rate of 5 mL/min. The radioactive peak corresponding to TZ7774 was corrected in a flask, evaporated to dryness in a rotary evaporator and dissolved in 3 mL of saline with 7.5 µL of Tween-80 filtered through a 0.22 µm Milex filter. The radiochemical purity, the chemical purity and the molar activity of [^{11}C]TZ7774 were analyzed by HPLC (column: CAPCELL PAK C18, UG120, 4.6 × 150 mm, UV = 260 nm) eluting with a 55% CH$_3$CN in 0.1% formic acid at a flow rate of 1.0 mL/min. [^{11}C]TZ7774 was reliably obtained 1336.6 ± 492.8 MBq in an 3.4 ± 1.2% decay-corrected radiochemical yield, a molar activity of 137.8 ± 54.3 GBq/µmol, with a chemical purity 82.3 ± 19.4 % and with a radiochemical purity > 99.9 % (n = 9).

References

[1] Huang T, Gu J, Jiang H, Liang Q, Perlmutter JS and Tu Z. Radiosynthesis and characterization of a carbon-11 PET tracer for receptor-interacting protein kinase 1. Nucl Med Biol 2022; 110-111: 18-27.

[2] Yoshikawa M, Saitoh M, Katoh T, Seki T, Bigi SV, Shimizu Y, Ishii T, Okai T, Kuno M, Hattori H, Watanabe E, Saikatendu KS, Zou H, Nakakariya M, Tatamiya T, Nakada Y and Yogo T. Discovery of 7-Oxo-2,4,5,7-tetrahydro-6 H-pyrazolo[3,4- c]pyridine derivatives as potent, orally available, and brain-penetrating receptor interacting protein 1 (RIP1) kinase inhibitors: analysis of structure-kinetic relationships. J Med Chem 2018; 61: 2384-2409.

[3] Sakai T, Ogata A, Ikenuma H, Yamada T, Hattori S, Abe J, Imamura S, Ichise M, Tada M, Kakita A, Koyama H, Suzuki M, Kato T, Ito K and Kimura Y. A novel PET probe to selectively image heat shock protein 90α/β isoforms in the brain. EJNMMI Radiopharm Chem 2024; 9: 19.

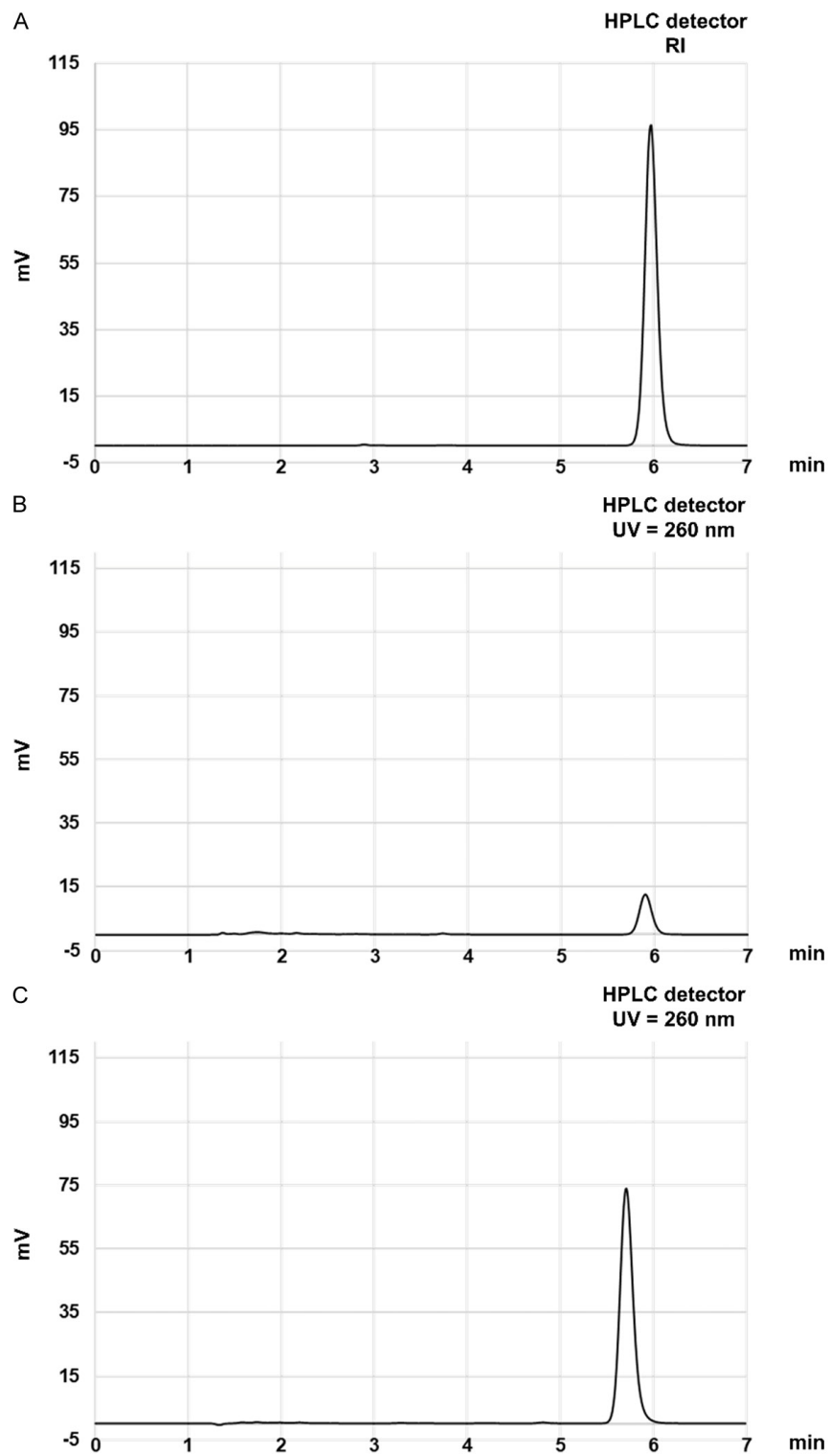# Specific binding of [¹¹C]TZ7774 to RIPK1 in the brain

Figure S1. HPLC chromatogram of [¹¹C]TZ7774 and TZ7774. [¹¹C]TZ7774 (A), TZ7774 (B) and [¹¹C]TZ7774 with TZ7774 was analyzed by HPLC (column: CAPCELL PAK C18, 4.6 × 150 mm, UG120) eluting with around 55% CH_3CN in 0.1% formic acid at a flow rate of 1.0 mL/min. HPLC peaks were detected with RI (A, rt, 5.95 min), UV (B, rt 5.84 min) and UV (C, rt 5.72 min).
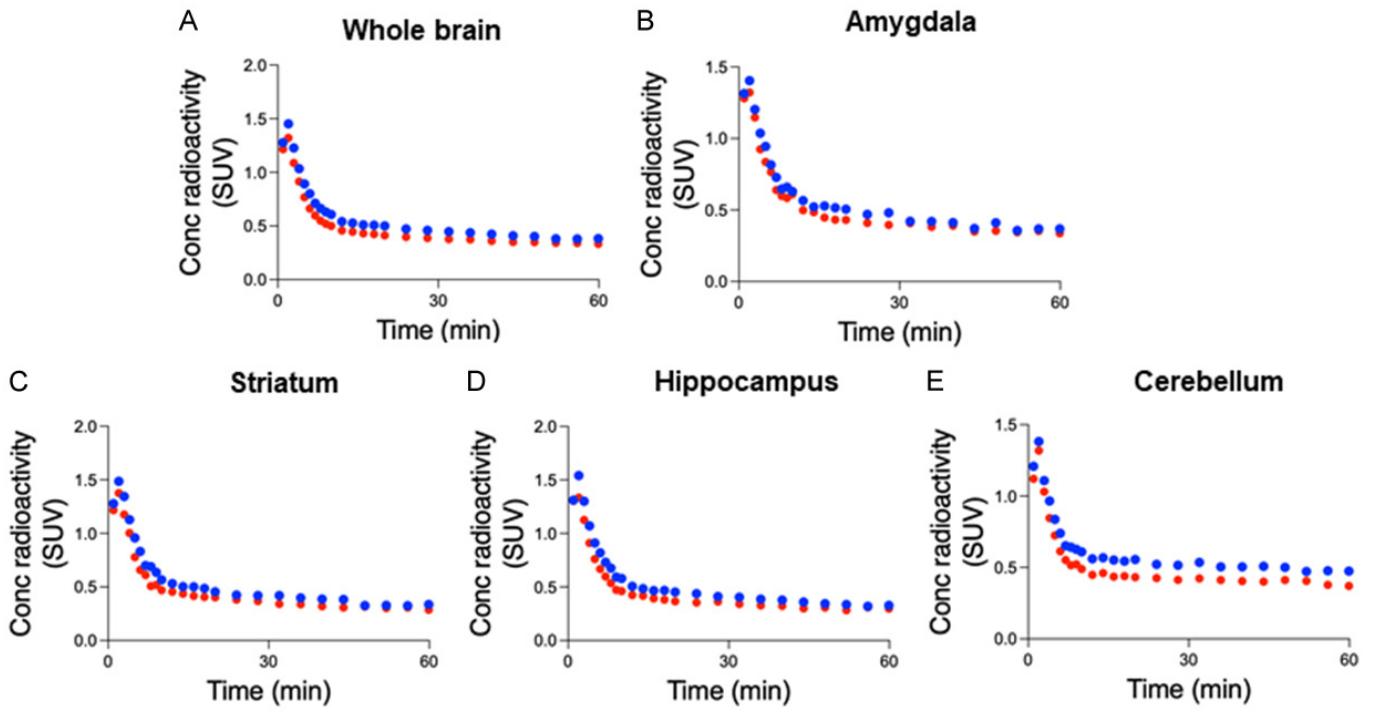
Figure S2. PET imaging study of [^{11}C]TZ7774 in rats includes averaged time-activity curves for different brain regions. The regions analyzed are: the whole brain (A), amygdala (B), striatum (C), hippocampus (D), and cerebellum (E). The data compare the results after injection of [^{11}C]TZ7774 with (blue circles) and without (red circles) the administration of 1 mg/kg of GSK'963 as a blocking agent.
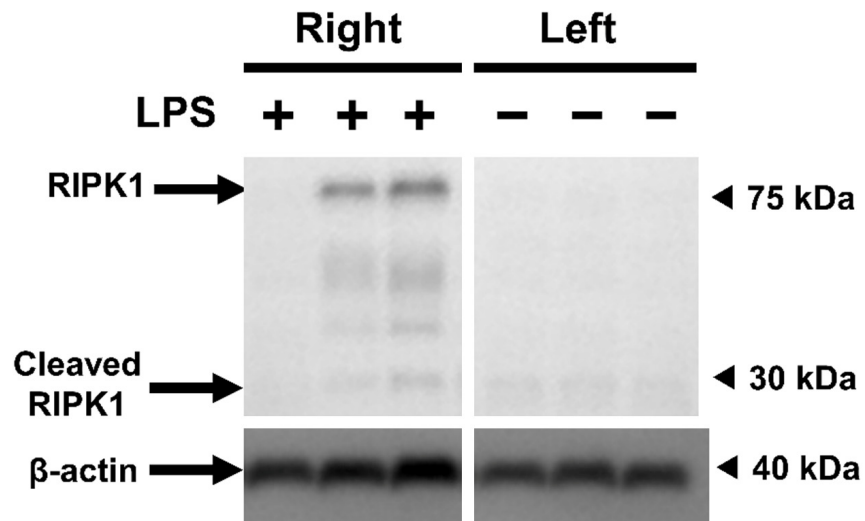

Figure S3. RIPK1 protein expression in homogenates of right and left striatum of rats injected with LPS (25 µg) in the right brain striatum.
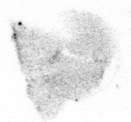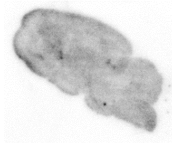
Specific binding of [^{11}C]TZ7774 to RIPK1 in the brain
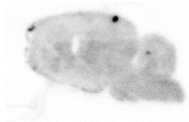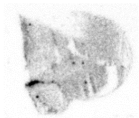

Figure S4. Autoradiography of a sagittal section of a healthy rat (A) and frontal sections of a healthy human (B), with or without the addition of GSK'963 (10 µM) as a blocking agent.